Investigating neutron transfer in the ^{9}Be + ^{197}Au system

Malika Kaushik,[1] S. K. Pandit,[2] V. V. Parkar,[2,4] G. Gupta,[3] Swati Thakur,[1] V. Nanal,[3] H. Krishnamoorthy,[4,5] A. Shrivastava,[2,4] C. S. Palshetkar,[3] K. Mahata,[2,4] K. Ramachandran,[2] S. Pal,[6] R. G. Pillay,[1] and Pushpendra P. Singh[1,*]

[1]*Department of Physics, Indian Institute of Technology Ropar, Rupnagar 140 001, Punjab, India*
[2]*Nuclear Physics Division, Bhabha Atomic Research Centre, Mumbai 400 085, India*
[3]*Department of Nuclear and Atomic Physics, Tata Institute of Fundamental Research, Mumbai 400 005, India*
[4]*Homi Bhabha National Institute, Anushaktinagar, Mumbai 400 094, India*
[5]*India-based Neutrino Observatory, Tata Institute of Fundamental Research, Mumbai 400 005, India*
[6]*Pelletron Linac Facility, Tata Institute of Fundamental Research, Mumbai 400 005, India*

(Received 28 April 2021; accepted 9 August 2021; published 24 August 2021)

In this work n-transfer and incomplete fusion cross sections for the ^{9}Be + ^{197}Au system are reported over a wide energy range, $E_{c.m.} \approx$ 29-45 MeV. The experiment was carried out using the activation technique and off-line γ counting. The transfer process is found to be the dominant mode as compared to all other reaction channels. Detailed coupled reaction channel (CRC) calculations have been performed for n-transfer stripping and pickup cross sections. The measured 1n-stripping cross sections are explained with CRC calculations by including the ground state and the 2^{+} resonance state (E = 3.03 MeV) of ^{8}Be. The calculations for 1n-pickup cross sections, including only the ground state of ^{10}Be agrees reasonably well with the measured cross sections, while it overpredicts the data at subbarrier energies. For better insight into the role of the projectile structure in the transfer process, a comprehensive analysis of the 1n-stripping reaction has been carried out for various weakly bound projectiles on a ^{197}Au target nucleus. The transfer cross sections scaled with the square of the total radius of interacting nuclei show the expected Q-value dependence of the 1n-stripping channel for weakly bound stable projectiles.

DOI: 10.1103/PhysRevC.104.024615

I. INTRODUCTION

The nuclear reactions involving weakly bound projectiles open up many distinctive facets of reaction dynamics and play a crucial role in understanding the interplay between quantum tunneling and the breakup process at energies around the Coulomb barrier [1]. The striking characteristics of weakly bound projectiles, e.g., low breakup threshold (E_{BU}) and underlying cluster structure, significantly affect nuclear dynamics [2,3]. The weakly bound projectiles like ^{6,7}Li and ^{9}Be can break up into their constituent clusters during the interaction process. As a consequence of the weak binding of the projectile, one of the projectile fragments following breakup can get absorbed by the target nucleus, known as breakup fusion [4–8]. Single step cluster transfer from the bound state of the projectile to bound/unbound states of the target is also one of the dominant mechanisms, as shown in recent studies [9–11]. These two processes are sometimes also referred to as incomplete fusion (ICF).

Complete fusion (CF) is defined as the amalgamation of the projectile as a whole with the target nucleus. It should be pointed out that CF and breakup followed by sequential capture of all the projectile fragments cannot be distinguished experimentally. In the case of weakly bound projectiles, it was suggested that the fusion suppression at the above-barrier energies occurs due to the direct breakup of the projectile, while the breakup following transfer is a dominant mechanism at subbarrier energies [12]. In several existing studies of ^{6,7}Li and ^{9}Be [8,13,14], the fusion suppression was attributed to the breakup of the projectile [13]. However, in a recent exclusive measurement, Cook *et al.* [9] have shown that the suppression of CF is primarily a consequence of strong clustering in weakly bound projectiles rather than the breakup prior to reaching the fusion barrier. These recent results emphasize the role of transfer reactions with weakly bound projectiles.

Investigation of the transfer channel measurements provides insight into low-energy reaction dynamics, particularly to understand the role of valence nucleons, the spatial correlations of the valence nucleons, and the pairing properties [15]. Relatively larger (1n and 2n) transfer cross sections have been observed in reactions involving halo projectiles (^{6,8}He) [15,16]. Several investigations with a stable weakly bound projectile, ^{9}Be [7,8,17,18], suggest that the neutron transfer channels dominate over CF at subbarrier energies. The CF excitation functions typically show a steeper fall off compared to the transfer channels [17]. In the ^{6}Li + ^{96}Zr [19] reaction, it has been reported that the neutron transfer channels contribute significantly to the total reaction cross section, especially at energies around the Coulomb barrier. In a ^{6}He + ^{64}Zn experiment, Pietro *et al.* [20] observed that

*pps@iitrpr.ac.in

transfer and breakup channels make up the largest fraction of the reaction cross section (about 80%) in the near-barrier region.

In a recent measurement of the ^{9}Be + ^{197}Au system [21], the fusion cross sections have been found to be suppressed by ∼39% with respect to theoretical calculations (CCFULL) at above-barrier energies. ^{9}Be, the Borromean nucleus, may break into $\alpha + \alpha + n$ ($E_{BU} = 1.57$ MeV) [22,23] or ^{8}Be $+n$ ($E_{BU} = 1.66$ MeV) or ^{5}He $+\alpha$ ($E_{BU} = 2.31$ MeV) [24]. ^{8}Be and ^{5}He are unbound with lifetimes of 10^{-16} and 10^{-21} s, respectively. In reactions with ^{9}Be, at energies around the Coulomb barrier, the $n + {}^{8}$Be cluster configuration has been shown to play a prominent role as compared to the ^{5}He $+\alpha$ configuration [7,18]. In this work, we have investigated neutron transfer and incomplete fusion in the ^{9}Be + ^{197}Au system at energies around the Coulomb barrier. It should be noted that, in inclusive measurements, contributions by the different mechanisms of breakup fusion and single step cluster transfer cannot be distinguished and are referred to as ICF in this paper. The experimental methodology and the analysis are presented in Sec. II. The detailed theoretical model calculations and their comparison with the experimental data of transfer channel cross sections in the ^{9}Be + ^{197}Au system are described in Sec. III. The analysis of transfer channel cross sections in the ^{9}Be + ^{197}Au system (present work) and the reactions involving other weakly bound projectiles, $x + {}^{197}$Au systems, are delineated in Sec. IV. The summary of the present work is outlined in Sec. V.

II. EXPERIMENTAL DETAILS AND DATA ANALYSIS

The experiment was performed using 30- to 47-MeV ^{9}Be beams from the BARC-TIFR Pelletron Linac Facility, Mumbai, India. A detailed description of the experimental setup and data analysis is given in Ref. [21]. Self-supporting ^{197}Au target foils (thickness ∼1.3-1.7 mg/cm^2) together with aluminum catcher foils (thickness ∼1.5 mg/cm^2) to stop recoiling products were used. Irradiation was done in 1- to 2-MeV steps with a beam current of 8–15 pnA. In some cases, stacked target-catcher foil assemblies were deployed, and the beam energy at the center of the target was calculated using SRIM [25]. The activity in the irradiated targets was measured using an off-line γ-ray counting method with efficiency-calibrated high-purity germanium detectors. The counting geometry, i.e., sample at a distance of 10 cm from the detector face or at the face, was chosen depending on the activity level in the sample. The transfer and ICF reaction products were identified by their characteristic γ rays. The identification was independently confirmed by half-life measurements.

Typical γ-ray spectra corresponding to $E_{lab} = 46.7$ and 36.6 MeV energies are shown in Fig. 1, where the γ rays corresponding to transfer ^{198}Au (1n-stripping), ^{196}Au (1n-pickup), and ICF (^{199}Tl, ^{200}Tl) products are marked. The measured reaction products of transfer and ICF in the ^{9}Be + ^{197}Au system are listed in Table I along with the most intense characteristic γ ray and the corresponding intensity. It may be noted that ^{199}Tl can be populated via either ^{197}Au(^{4}He, 2n) or ^{197}Au(^{5}He, 3n) reactions. Similarly, both

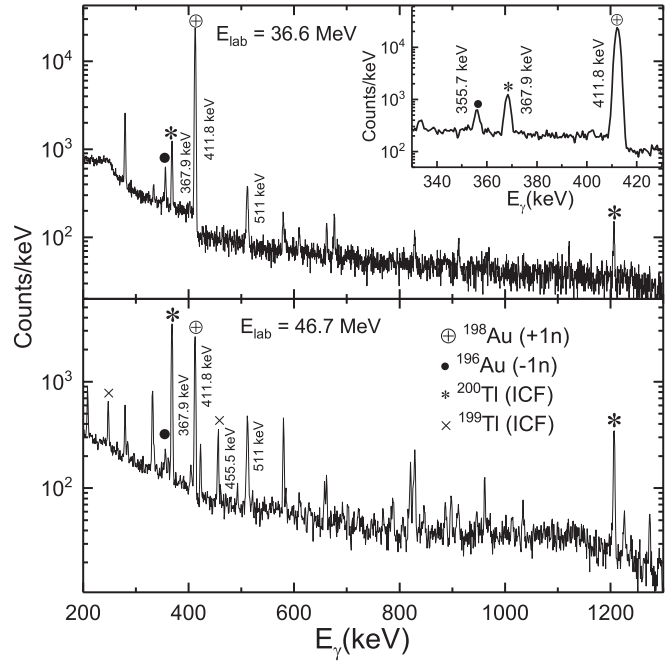

FIG. 1. Typical γ-ray spectra of the ^{9}Be + ^{197}Au system measured at $E_{lab} = 36.6$ MeV ($t_{collection} = 11.1$ h) and 46.7 MeV ($t_{collection} = 1.55$ h), recorded after a cooldown period of 4.64 and 0.71 days, respectively. Some of intense decay γ lines corresponding to different reaction products are marked.

^{197}Au(^{4}He, 1n) and ^{197}Au(^{5}He, 2n) contribute to the production of ^{200}Tl.

The cross sections for the reaction products populated due to transfer and ICF channels are extracted from the photopeak yields of characteristic γ rays by taking into account the decay during the irradiation [21]. The measured cross sections at different energies are listed in Table II and plotted in Fig. 2. It should be mentioned that the quoted errors include statistical and fitting errors.

III. RESULTS AND DISCUSSION

Excitation functions for reaction products populated due to 1n-stripping (^{198}Au) and 1n-pickup (^{196}Au) and to ICF followed by neutron evaporation (^{199,200}Tl) are shown in Figs. 2(a) and 2(b), respectively. The value of the barrier ($V_B = 38.4$ MeV) [21] is shown by an arrow. As shown in Fig. 2, the transfer component is measured down to ≈29 MeV

TABLE I. List of reaction products populated via transfer and ICF channels in the ^{9}Be + ^{197}Au system with respective half-life ($T_{1/2}$) together with energy and absolute intensity (I_γ) of the most intense characteristic γ ray [26].

Reaction	Nuclide	$T_{1/2}$	E_γ (keV)	I_γ (%)
1n-stripping	^{198}Au	2.69 d	411.8	95.6
1n-pickup	^{196}Au	6.17 d	355.7	87.0
ICF	^{200}Tl	26.1 h	367.9	87.0
ICF	^{199}Tl	7.42 h	455.5	12.4

TABLE II. Experimentally measured cross sections of ICF (^{200,199}Tl) evaporation residues and transfer (^{198,196}Au) channels populated in the ^{9}Be + ^{197}Au system (V_B = 38.4 MeV).

E_{lab} (MeV)	$E_{c.m.}$ (MeV)	^{200}Tl (mb)	^{199}Tl (mb)	^{198}Au (mb)	^{196}Au (mb)
30.4	29.1	–	–	11.2 ± 0.1	–
33.0	31.6	0.150 ± 0.002	–	24.3 ± 0.2	0.150 ± 0.006
34.5	33.0	0.76 ± 0.01	–	33.2 ± 0.2	0.35 ± 0.03
35.6	34.0	3.50 ± 0.05	–	69.3 ± 0.4	0.90 ± 0.07
36.6	35.0	10.5 ± 0.09	–	83.7 ± 0.3	1.30 ± 0.08
37.6	36.0	22.5 ± 0.2	0.5 ± 0.2	124.2 ± 0.6	2.6 ± 0.3
38.6	36.9	36.6 ± 0.5	2.6 ± 0.6	123.8 ± 0.8	3.5 ± 0.4
39.6	37.9	55.2 ± 0.4	5.2 ± 0.9	135.4 ± 0.6	5.8 ± 0.6
39.9	38.2	68.0 ± 0.6	10.6 ± 1.5	139.7 ± 1.4	5.2 ± 0.7
40.6	38.8	92.1 ± 0.8	11.0 ± 1.2	189.6 ± 1.4	6.6 ± 0.8
42.7	40.8	95.7 ± 0.8	20.3 ± 1.9	154.1 ± 1.3	7.2 ± 0.7
44.7	42.7	144.3 ± 1.3	56.5 ± 2.8	164.7 ± 1.4	8.5 ± 0.6
46.7	44.7	119.1 ± 1.2	75.4 ± 5.1	136 ± 1	9.1 ± 0.4

(i.e., ≈24% below the barrier), while the incomplete fusion component is measured down to ≈18% below the barrier. To get a comprehensive picture of CF [21], ICF, and transfer reactions, cross sections of all these channels are plotted as a function of energy in Fig. 3. As can be seen from this figure, the transfer process significantly dominates over CF and ICF processes at subbarrier energies, whereas CF shows higher cross sections at above-barrier energies.

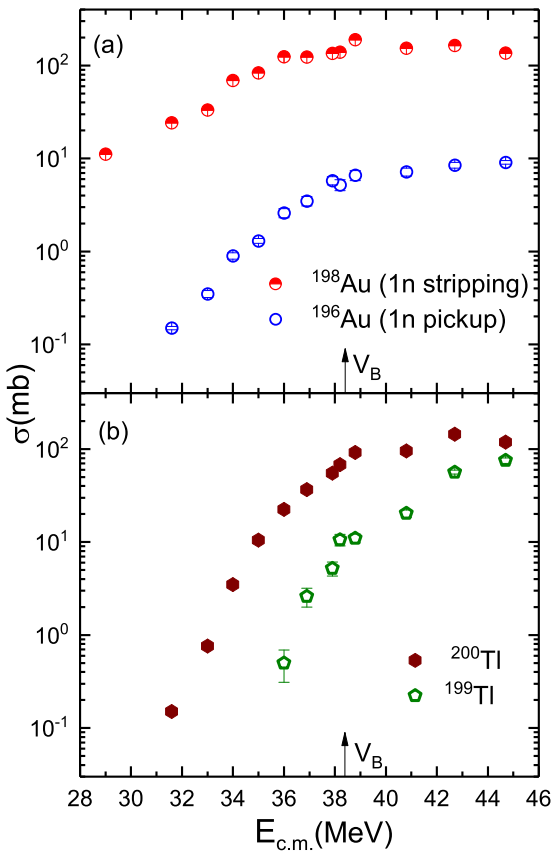

FIG. 2. Measured excitation functions of (a) transfer (^{198,196}Au) and (b) ICF (^{200,199}Tl) channels populated in the ^{9}Be + ^{197}Au system. The barrier value (V_B = 38.4 MeV) is marked on the energy axis.

Coupled reaction channel calculations: ^{9}Be + ^{197}Au system

For further analysis of the transfer channels presented in Fig. 2, the coupled reaction channel (CRC) calculations have been performed using a theoretical model code FRESCO [27]. For CRC calculations, optical model potentials for entrance and exit channels, binding potentials between transferred particle and core nucleus, and spectroscopic factors for different residual states are required inputs. The optical model potential is usually taken to be of Woods-Saxon form for both real and imaginary parts. The potential parameters for n + ^{197}Au are taken to be the same as those of n + ^{208}Pb from Ref. [28], because ^{197}Au and ^{208}Pb lie in similar mass regions.

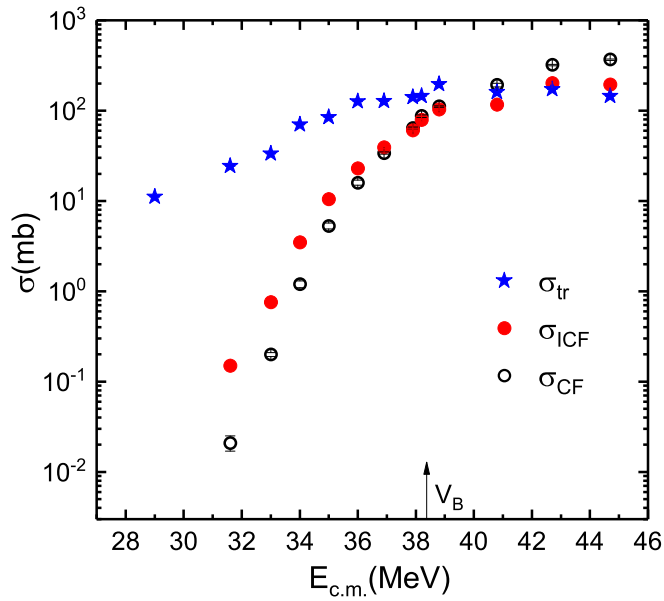

FIG. 3. Comparison of measured transfer, ICF, and CF [21] cross sections as a function of $E_{c.m.}$ in the ^{9}Be + ^{197}Au system.

TABLE III. Potential parameters used in CRC calculations for ^{9}Be + ^{197}Au and ^{6,7}Li + ^{197}Au systems. The radius parameters in the potentials are derived from $R_i = r_i \cdot A^{1/3}$, where $i = R, V, S$, and C, and A is the target mass number.

System	V_R (MeV)	r_R (fm)	a_R (fm)	W_V(MeV)	r_V (fm)	a_V (fm)	W_S(MeV)	r_S (fm)	a_S (fm)	r_C (fm)
$n + ^{197}$Au [28]	50.00[a]	1.23	0.65	–	–	–	6.00	1.23	0.65	–
$2n + ^{197}$Au [28]	50.00[a]	1.23	0.65	–	–	–	6.00	1.23	0.65	–
$n + ^{196}$Au [28]	50.00[a]	1.23	0.65	–	–	–	6.00	1.23	0.65	–
$n + ^{8}$Be [29]	50.00[a]	1.15	0.57	–	–	–	5.50	1.15	0.57	–
$n + ^{9}$Be [29]	50.00[a]	1.15	0.57	–	–	–	5.50	1.15	0.57	–
^{9}Be + ^{197}Au [30]	257.70	1.36	0.73	16.32	1.64	0.60	46.30	1.20	0.84	1.56
$n + ^{7}$Li [33]	50.00[a]	1.25	0.70	–	–	–	6.00	1.25	0.70	–
$n + ^{6}$Li [33]	50.00[a]	1.25	0.70	–	–	–	6.00	1.25	0.70	–
$2n + ^{5}$Li [33]	50.00[a]	1.25	0.70	–	–	–	6.00	1.25	0.70	–
^{6}Li + ^{197}Au [33]	109.50	1.33	0.81	20.71	1.53	0.88	–	–	–	1.30
^{7}Li + ^{197}Au [33]	114.20	1.29	0.85	20.71	1.74	0.81	–	–	–	1.30

[a]Depth adjusted to obtain the correct binding energy.

Because an $n + ^{8}$Be cluster picture of ^{9}Be has been used in the present analysis, the potential parameters of the binding of n in the ^{9}Be projectile, i.e., the depth of volume potential, the radius, and the diffuseness along with the spin-orbit component, are taken from Ref. [29]. The global optical model potential parameters for the ^{9}Be + ^{197}Au system are taken from Ref. [30]. These potential parameters are further cross-checked by reproducing the experimentally measured elastic scattering cross sections for this system over a wide energy range, $E_{\text{c.m.}} = 32.5$-46 MeV [31].

The optical model potential parameters for 1n-stripping (^{198}Au) and 1n-pickup (^{196}Au) channel calculations are given in Table III. In 1n-stripping, the spectroscopic factor (C^2S) for ^{9}Be / ^{8}Be is taken to be 0.42 [29] and 1 for the ground state and 2^+ resonance state of ^{8}Be, respectively. In 1n-pickup, C^2S for ^{9}Be / ^{10}Be is taken to be 1.58 [32]. For both 1n-stripping and 1n-pickup, the spectroscopic factors for target states have been set to 1.0. From the number of ^{198}Au excited states up to 1.560 MeV given in Ref. [26], only those states with J values less than 5 and well-determined J^π values have been considered. Further, the calculations have been performed with a limited number of states at a time, at three experimental energy points, viz., the highest ($E_{\text{c.m.}} = 44.7$ MeV), lowest ($E_{\text{c.m.}} = 33$ MeV), and barrier ($E_{\text{c.m.}} = 38.2$ MeV) energies. This procedure has been used to select the states that dominantly contribute to the 1n-transfer channel and are listed in Table IV. For all the beam energies, the final CRC calculations have been performed including these states. Similarly, the excited states of ^{196}Au up to 0.388 MeV having J values less than 5 and well-determined J^π values have been considered as listed in Table IV. The couplings of ^{198}Au excited states, as given in Table IV, have been included along with the 0^+ ground state and the 2^+ resonance state of ^{8}Be. The inelastic states of the projectile (^{9}Be) and the target (^{197}Au) have not been included in the present calculations.

The excitation functions of (a) 1n-stripping (^{198}Au) and (b) 1n-pickup (^{196}Au) channels in the ^{9}Be + ^{197}Au system along with the calculations are shown in Fig. 4. As can be seen from the figure, the calculations including couplings only to the ground state of ^{8}Be underpredict the $\sigma_{1n\text{-stripping}}$ over the entire measured energy range, while those with couplings to both the ground state and the 2^+ resonance state of ^{8}Be well describe the data. It is evident that the 2^+ resonance state plays a crucial role in the 1n-stripping channel. The $Q_{\text{opt}} = 0$ for n-transfer using the semiclassical expression given in Ref. [34]. The inclusion of the 2^+ resonance state of ^{8}Be at 3.03 MeV provides a better matching with the Q value in

TABLE IV. Energy levels of transfer products used in the CRC calculations in the ^{6,7}Li + ^{197}Au and ^{9}Be + ^{197}Au systems [26].

^{199}Au		^{198}Au		^{196}Au	
E (MeV)	J^π	E (MeV)	J^π	E (MeV)	J^π
0.0	1.5^+	0.0	2^-	0.0	2^-
0.077	0.5^+	0.215	4^-	0.006	1^-
0.317	2.5^+	0.381	3^+	0.213	4^-
0.323	1.5^+	0.544	4^-	0.234	3^-
0.493	3.5^+	0.764	4^-	0.324	1^-
0.543	2.5^+	0.825	3^+	0.326	1^-
0.549	5.5^-	0.869	3^-	0.349	2^-
0.735	3.5^-	0.972	3^-	0.375	3^-
0.791	1.5^+	1.032	3^-	0.388	3^+
0.822	0.5^+	1.061	3^-		
0.907	1.5^+	1.115	3^-		
1.801	1.5^+	1.157	3^-		
2.107	0.5^+	1.160	3^-		
2.205	0.5^+	1.209	3^-		
2.412	0.5^+	1.240	3^-		
2.734	0.5^+	1.272	3^-		
		1.305	3^-		
		1.381	3^-		
		1.396	3^-		
		1.409	3^-		
		1.424	3^-		
		1.444	3^-		
		1.454	3^-		
		1.459	3^-		
		1.472	3^-		
		1.496	3^-		
		1.560	3^-		

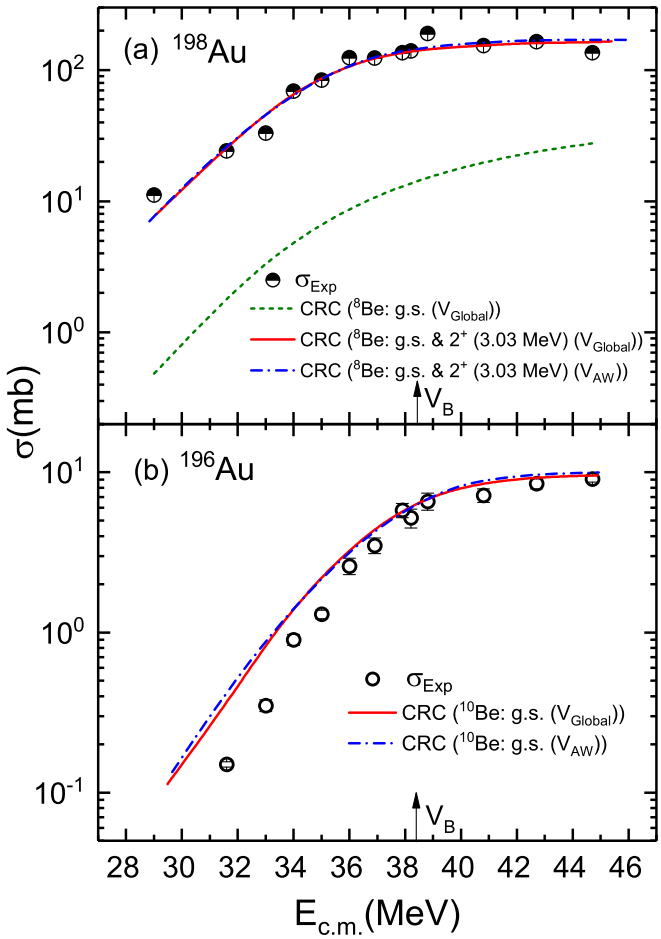

FIG. 4. Comparison of measured excitation functions with CRC calculations of transfer channels for (a) ^{198}Au including the ground state and the 2^{+} resonance (E = 3.03 MeV) state of ^{8}Be, and only the ground state of ^{8}Be, and (b) ^{196}Au with the ground state of ^{10}Be using the global optical potential (V_{Global}). The dash-dotted lines represent the CRC calculations with the Akyuz-Winther (V_{AW}) potential in both of the transfer channels.

the 1n-stripping reaction. In the case of ^{196}Au, the couplings to excited states of ^{196}Au as given in Table IV and the 0^{+} ground state of ^{10}Be have been included in the calculations. As shown in Fig. 4(b), the calculations for ^{196}Au agree reasonably well with the experimental data, but overpredict at subbarrier energies. It should be mentioned that the CRC calculations performed with the Akyuz-Winther (AW) potential [21], for both real and imaginary parts, also describe the data fairly well as shown in Fig. 4. It may be noted that ^{198}Au cross sections are significantly larger than ^{196}Au cross sections. In principle, ^{198}Au can also have contributions from ICF. However, the observed good agreement with CRC calculations indicates that the dominant contribution arises from the transfer process.

IV. TRANSFER REACTION SYSTEMATICS IN $x + ^{197}$Au SYSTEMS

For a comprehensive understanding of the projectile structure effect on transfer reactions, it is useful to carry out a systematic comparison for transfer cross sections (σ_{tr}) of various weakly bound stable projectiles, i.e., ^{6,7}Li, ^{9}Be, and ^{10}B with a ^{197}Au target. For comparison with transfer reactions of other weakly bound stable projectiles, namely, ^{6,7}Li [35], the experimental excitation functions have been analyzed in the framework of CRC calculations following a procedure similar to that described in the previous section.

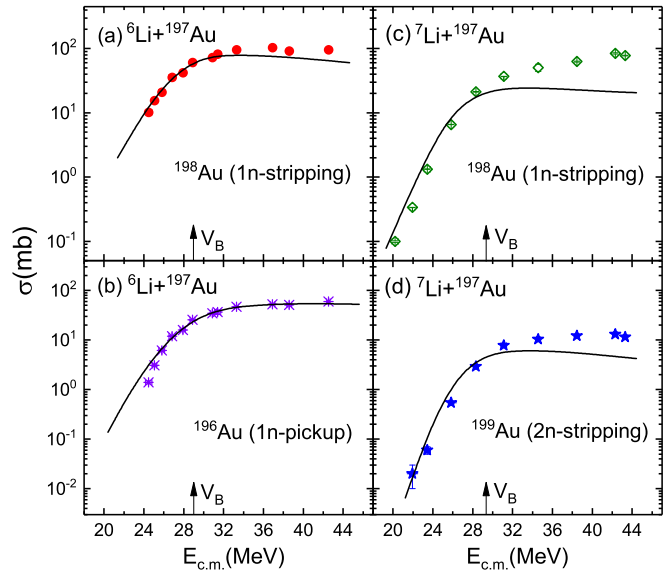

FIG. 5. Comparison of measured cross sections [35]: (a) 1n-stripping and (b) 1n-pickup in the ^{6}Li + ^{197}Au (V_B = 28.9 MeV) system and (c) 1n-stripping and (d) 2n-stripping in the ^{7}Li + ^{197}Au (V_B = 29.3 MeV) system with CRC calculations (solid curve). The Coulomb barrier (V_B) is marked by arrows.

A. CRC calculations: ^{6,7}Li + ^{197}Au systems

The excitation functions of transfer reaction products, ^{196}Au, ^{198}Au, and ^{199}Au, in ^{6,7}Li + ^{197}Au [35] systems are presented in Fig. 5. The global optical potential parameters used in the calculation are presented in Table III. The potential parameters V_R, W_V, and W_S parameter denote the V_0, W_0, and V_S parameters in the ^{6,7}Li + ^{197}Au systems which are quoted in Ref. [33]. In the case of the ^{6}Li + ^{197}Au system, the ^{6}Li / ^{5}Li and ^{6}Li / ^{7}Li spectroscopic factors are taken to be 1.12 and 1.85 for 1n-stripping and 1n-pickup channels, respectively [32]. Similar to the ^{9}Be + ^{197}Au system, spectroscopic factors for target states (^{196,198}Au) have been fixed at 1.0. In 1n-stripping calculations, the couplings of ^{198}Au excited states up to 1.240 MeV as tabulated in Table IV and the 3/2^{-} ground state of ^{5}Li have been included.

As shown in Fig. 5(a), the CRC calculations for 1n-stripping (^{198}Au) agree well with experimental data at subbarrier energies and underpredict at above-barrier energies. Figure 5(b) shows the CRC calculations for the 1n-pickup channel, performed by including couplings of ^{196}Au excited states up to 0.388 MeV given in Table IV and the 3/2^{-} ground state of ^{7}Li. It can be seen that the measured excitation function of the 1n-pickup channel is well reproduced

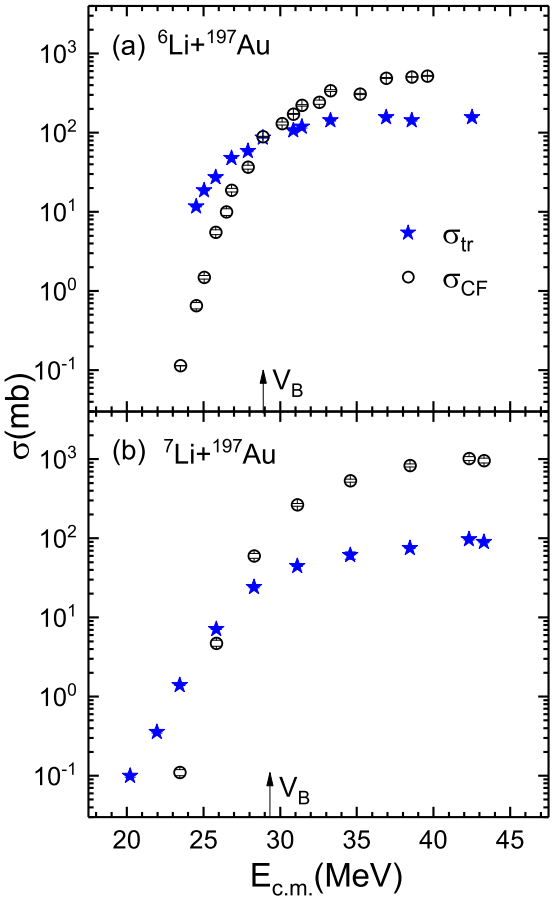

FIG. 6. Comparison of the measured excitation functions of CF and transfer reaction in (a) ^{6}Li + ^{197}Au and (b) ^{7}Li + ^{197}Au systems [35], where V_B is the barrier.

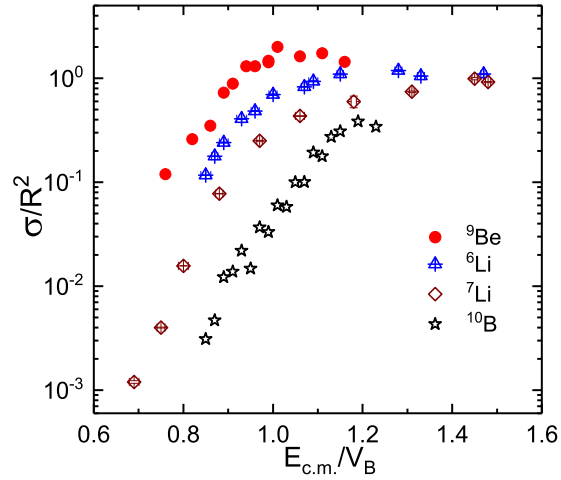

FIG. 7. Comparison of measured transfer excitation functions of the 1n-stripping (^{198}Au) channel in ^{9}Be + ^{197}Au (present work) and other reactions, x + ^{197}Au, involving ^{7}Li [35], ^{6}Li [35], and ^{10}B [37] projectiles.

by the CRC calculations except for the lowest energy below the barrier.

A similar analysis has been carried out for the ^{7}Li + ^{197}Au system and is presented in Figs. 5(c) and 5(d). For CRC calculations of the 1n-stripping channel (^{198}Au), the ^{7}Li / ^{6}Li and ^{197}Au / ^{198}Au spectroscopic factors have been taken to be 1.85 [32] and 1.0, respectively. The couplings of ^{198}Au excited states up to 0.972 MeV are listed in Table IV and the 1^+ ground state of ^{6}Li has been included in the CRC calculations. Similarly, for the 2n-stripping channel (^{199}Au), the couplings of ^{199}Au excited states up to 2.734 MeV are listed in Table IV and the $3/2^-$ ground state of ^{5}Li has been included. All the ^{199}Au excited states with well-determined J^π values have been considered. The ^{7}Li / ^{5}Li and ^{197}Au / ^{199}Au spectroscopic factors have been taken as 1.0 in the calculations. As shown in Figs. 5(c) and 5(d), the CRC calculations show a reasonable agreement with the experimental data at subbarrier energies and underpredict the data at above-barrier energies. The increasing trend of underprediction of CRC calculations at above-barrier energies indicates the involvement of more states (high excitation energy) of targetlike nuclei, which could not be included in the present calculations.

As an illustration of the influence of the projectile structure in transfer reactions, a systematic comparison of σ_{tr} with CF cross sections (σ_{CF}) [35] for subbarrier to above-barrier energies has been carried out for ^{6,7}Li + ^{197}Au systems and is shown in Fig. 6. It can be seen that for both ^{6}Li and ^{7}Li projectiles σ_{tr} is higher than σ_{CF} at subbarrier energies as expected. The σ_{tr}/σ_{CF} for ^{6}Li is larger than that for ^{7}Li, but is considerably smaller than that for ^{9}Be (refer to Fig. 3). This enhancement of transfer cross section over CF may be attributed to the structural differences of ^{6,7}Li and ^{9}Be projectiles. In ^{9}Be the last valence neutron has a large spatial extension [4] and the coupling to the 2^+ resonant state in ^{8}Be plays a crucial role.

B. Comparison of transfer cross sections in x + ^{197}Au systems

The excitation functions of the 1n-stripping channel with different weakly bound stable projectiles ^{6,7}Li, ^{9}Be (present work), and ^{10}B on a ^{197}Au target are compared in Fig. 7 with suitable scaling. To suppress trivial differences that arise due to the geometrical effects of the interacting nuclei, a simple semiclassical scaling procedure used in Ref. [36] for fusion cross section comparison is adopted for the transfer cross

TABLE V. List of dominant breakup channels together with corresponding breakup threshold energy (E_{BU}) and ground-state Q values for 1n-stripping ($Q_{1n\text{-strip}}$) and 1n-pickup ($Q_{1n\text{-pickup}}$) reactions in MeVs for weakly bound projectiles considered in the present study.

Nuclei	Channel	E_{BU} (MeV)	$Q_{1n\text{-strip}}$	$Q_{1n\text{-pickup}}$
^{9}Be	$\alpha + \alpha + n$	1.57	4.85	−1.26
	^{8}Be + n	1.66		
^{7}Li	$\alpha + t$	2.47	−0.74	−6.04
^{6}Li	$\alpha + d$	1.47	0.85	−0.82
^{10}B	^{6}Li + α	4.46	−1.92	3.38
	^{9}B + n	8.44		

TABLE VI. Radii of different projectiles in $x + {}^{197}$Au systems.

Projectile	R_P (fm)	Ref.
^{6}Li	2.09	[38]
^{7}Li	2.23	[38]
^{9}Be	2.45	[38]
^{10}B	1.95	[39]

section. The scaled parameters are defined as

$$\sigma_{sc} = \sigma/R^2 \quad \text{and} \quad E_{sc} = E_{cm}/V_B, \tag{1}$$

where $R = R_P + R_T$ [R_P is the projectile radius and $R_T = 7.27$ fm ($1.25.A_T^{1/3}$) is the target nucleus radius] and V_B is the barrier. The V_B value for the ^{6,7}Li + ^{197}Au and ^{9}Be + ^{197}Au systems is taken from the CCFULL calculations, while that for the ^{10}B + ^{197}Au system is taken from Ref. [37]. The R_P values of different projectiles are listed in Table VI.

The projectile breakup thresholds (E_{BU}) and 1n-stripping Q values are tabulated in Table V. It can be seen from Fig. 7 and Table V that, amongst the weakly bound stable projectiles, σ_{sc} is the lowest for ^{10}B, which has the largest negative Q value, and is the highest for ^{9}Be, which corresponds to the largest positive Q value. Further, it should be mentioned that the choice of R_P is not crucial in the analysis, because σ scaled with R_B^2 (where R_B is the barrier radius obtained from CCFULL calculations) also shows a similar trend.

V. SUMMARY AND CONCLUSIONS

In summary, the transfer and ICF reaction cross sections have been measured in the ^{9}Be + ^{197}Au system in an energy range of $0.76 \leqslant E_{c.m.}/V_B \leqslant 1.16$ and analyzed using coupled reaction channel (CRC) calculations. The experimental excitation function of ^{198}Au populated via the 1n-stripping channel is well reproduced with the CRC calculations using couplings to the ground state and the 2^+ resonance state of ^{8}Be. It is shown that the 2^+ resonance state of ^{8}Be plays a significant role in the 1n-stripping channel. For the 1n-pickup channel, the CRC calculations including only the ground state of ^{10}Be are in reasonable agreement with the data at above-barrier energies, but overpredict the measured cross sections at subbarrier energies. The CRC calculations employing the Akyuz-Winther potential also describe the measured cross-section data of ^{198,196}Au reasonably well. A systematic analysis of 1n-transfer, CF, and ICF reaction channels shows the dominance of 1n-transfer over ICF and CF at subbarrier energies in the ^{9}Be + ^{197}Au system.

Additionally, the CRC calculations have been performed to analyze the excitation functions of transfer channels in ^{6,7}Li + ^{197}Au systems [35]. In the ^{6}Li + ^{197}Au system, it has been found that the CRC calculations for the 1n-stripping channel agree well with the experimental data at subbarrier energies but underpredict at above-barrier energies, while the 1n-pickup channel shows excellent agreement over most of the measured energy range. The calculations of 1n- and 2n-stripping transfer channels populated in the ^{7}Li + ^{197}Au system [35] agree well with the experimental data at subbarrier energies.

In the systematics for transfer reactions, the projectile structure effect is illustrated by comparison of 1n-stripping cross sections of ^{6,7}Li and ^{9}Be projectiles on ^{197}Au targets. The scaled excitation functions of 1n-stripping cross sections in the $x + {}^{197}$Au systems show the highest cross-section values for the ^{9}Be projectiles, as expected from the ground-state Q-value systematics for the weakly bound stable projectiles.

ACKNOWLEDGMENTS

We thank the PLF staff for providing the steady and smooth beam during the experiments and the target laboratory personnel for their help in the target preparation. We acknowledge the support of the Department of Atomic Energy, Government of India, under Project No. 12P-R&D-TFR-5.02-0300.

[1] V. Jha *et al.*, Phys. Rep. **845**, 1 (2020), and the references therein.
[2] L. F. Canto *et al.*, Phys. Rep. **424**, 1 (2006); **596**, 1 (2015), and the references therein.
[3] B. B. Back, H. Esbensen, C. L. Jiang, and K. E. Rehm, Rev. Mod. Phys. **86**, 317 (2014), and the references therein.
[4] C. Signorini, Eur. Phys. J. A **13**, 129 (2002).
[5] D. H. Luong, M. Dasgupta, D. J. Hinde, R. du Rietz, R. Rafiei, C. J. Lin, M. Evers, and A. Diaz-Torres, Phys. Lett. B **695**, 105 (2011); Phys. Rev. C **88**, 034609 (2013).
[6] B. R. Fulton *et al.*, Phys. Rev. C **70**, 047602 (2004).
[7] V. V. Parkar, V. Jha, S. K. Pandit, S. Santra, and S. Kailas, Phys. Rev. C **87**, 034602 (2013).
[8] R. Rafiei, R. du Rietz, D. H. Luong, D. J. Hinde, M. Dasgupta, M. Evers, and A. Diaz-Torres, Phys. Rev. C **81**, 024601 (2010).
[9] K. J. Cook, E. C. Simpson, L. T. Bezzina, M. Dasgupta, D. J. Hinde, K. Banerjee, A. C. Berriman, and C. Sengupta, Phys. Rev. Lett. **122**, 102501 (2019).
[10] K. J. Cook, E. C. Simpson, D. H. Luong, S. Kalkal, M. Dasgupta, and D. J. Hinde, Phys. Rev. C **93**, 064604 (2016).
[11] J. Lei and A. M. Moro, Phys. Rev. Lett. **123**, 232501 (2019).
[12] M. Dasgupta *et al.*, Nucl. Phys. A **834**, 147c (2010).
[13] M. Dasgupta *et al.*, Phys. Rev. C **66**, 041602(R) (2002).
[14] S. Kailas *et al.*, Nucl. Phys. A **834**, 155c (2010).
[15] A. Lemasson *et al.*, Phys. Rev. C **82**, 044617 (2010).
[16] A. Navin *et al.*, Phys. Rev. C **70**, 044601 (2004).
[17] Y. D. Fang *et al.*, Phys. Rev. C **93**, 034615 (2016).
[18] S. K. Pandit *et al.*, Phys. Rev. C **84**, 031601(R) (2011).
[19] S. P. Hu *et al.*, Phys. Rev. C **93**, 014621 (2016).
[20] A. Di. Pietro *et al.*, Phys. Rev. C **69**, 044613 (2004).
[21] M. Kaushik *et al.*, Phys. Rev. C **101**, 034611 (2020), and the references therein.
[22] P. Papka *et al.*, Phys. Rev. C **75**, 045803 (2007).
[23] T. A. D. Brown *et al.*, Phys. Rev. C **76**, 054605 (2007).
[24] N. Keeley, K. W. Kemper, and K. Rusek, Phys. Rev. C **64**, 031602(R) (2001); N. Keeley, A. Alamanos, K. Rusek, and K. W. Kemper, *ibid.* **71**, 014611 (2005).

[25] SRIM, http://www.srim.org
[26] National Nuclear Data Center (NNDC), https://www.nndc.bnl.gov
[27] I. J. Thompson, Comput. Phys. Rep. C **7**, 167 (1988).
[28] D. G. Kovar *et al.*, Nucl. Phys. A **231**, 266 (1974).
[29] J. Lang, R. Muller, J. Unternahrer, L. Jarczyk, B. Kamys, and A. Strzalkowski, Phys. Rev. C **16**, 1448 (1977).
[30] Y. Xu, Y. Han, H. Liang, Z. Wu, H. Guo, and C. Cai, Phys. Rev. C **99**, 034618 (2019).
[31] F. Gollan *et al.*, Nucl. Phys. A **1000**, 121789 (2020).
[32] M. B. Tsang, J. Lee, and W. G. Lynch, Phys. Rev. Lett. **95**, 222501 (2005).
[33] J. Cook, Nucl. Phys. A **388**, 153 (1982).
[34] W. Henning *et al.*, Phys. Rev. C **17**, 2245(R) (1978).
[35] C. S. Palshetkar *et al.*, Phys. Rev. C **89**, 024607 (2014).
[36] P. R. S. Gomes, J. Lubian, I. Padron, and R. M. Anjos, Phys. Rev. C **71**, 017601 (2005).
[37] M. Aversa *et al.*, Phys. Rev. C. **101**, 044601 (2020).
[38] I. Tanihata, H. Hamagaki, O. Hashimoto, Y. Shida, N. Yoshikawa, K. Sugimoto, O. Yamakawa, T. Kobayashi, and N. Takahashi, Phys. Rev. Lett. **55**, 2676 (1985).
[39] K. C. C. Pires, S. Appannababu, R. Lichtenthaler, and O. C. B. Santos, Phys. Rev. C **98**, 014614 (2018).